Babeș-Bolyai University

Faculty of Physics

Doctoral School of Physics

Doctoral Thesis Summary

DESIGNING PLASMONIC NANOSTRUCTURES FOR BIOSENSING APPLICATIONS BY OPTICAL SPECTROSCOPY

Tié Bi Djè Leopold

Scientific Advisor

Prof. Univ. Dr. Simion Aștilean

CLUJ-NAPOCA

2021

Table of Content

INTRODUCTION

This thesis is focused on the investigation of new plasmonic nanostructures, starting from design and fabrication toward characterization and validation of their capacity of detection of relevant biomolecules and bacterial agents by means of optical spectroscopy, in particular Surface-Enhanced Raman Scattering (SERS) and Localized Surface Plasmon Resonance (LSPR). Thus, this thesis is structured as following:

Chapter 1 presents a historical perspective of gold nanoparticles history. It also details their outstanding optical properties arisen from particular shapes such spheres and rods. We start by putting a particular accent on that called localized surface plasmon resonance (LSPR) such important phenomenon. Based on such phenomenon, we give details concerning light interaction with nanoparticle by absorption, scattering and extinction. Finally, we spread out their potential biomedical applications.

Chapter 2 presents an overview of vibrational spectroscopy and discuss the origin of Raman and SERS effects. Raman scattering complementary to infrared absorption spectroscopy in characterization of molecular vibrational transitions. Fabrication of SERS substrates by chemical sythesis routes and self-assembly methods with emphasis on nanorods are presented together with relevant applications in literature.

Chapter 3 brings to the fore fabrication of gold nanorods (AuNRs) performed in a two-steps process: firstly, we proceeded with gold (Au) "seeds" preparation followed by the growth of AuNRs in solution. The as-obtained colloidal AuNRs were characterized by the LSPR response through UV-vis spectrophotometer and transmission electron microscopy (TEM) image of as-synthesis AuNRs. Next, we have proceeded by building end-to-end assembly with cysteine as a molecular linker. In the other words, we made linear assembly of AuNRs. To reach our goal, we changed first the medium to more acidic reaching pH=3.1 and functionalized by cysteine in order to generate some nanochains. We have recorded in time the formation of the nanochains and observed the as-obtained nanochains according to the length. Actually, we have significantly succeeded to produce new formed NIR plasmonic band which continues to shift to the red compared with the one recorded after half hour. Consequently, the growth mechanism of the self-assembled AuNRs can be easily tuned, generating unique plasmonic responses characteristic of different assembling rates. Furthermore, the formation of linear end-to-end assemblies *via* interparticle hydrogen bonding between cysteine linkers was confirmed not only experimentally by the occurrence of the specific NIR plasmonic band and by TEM examination

of AuNRs assemblies, but also theoretically by finite-difference time-domain (FDTD) numerical simulations. Finally, a much higher electric field in the gaps between linked nanoparticles was subsequently demonstrated by SERS detection of molecules with enhancement factor better than of individual AuNRs.

The first part of **Chapter 4** presents the fabrication and characterization of a versatile biocompatible plasmonic nanoplatform based on a Whatman paper incorporating positively charged gold spherical nanoparticles *via* the immersion approach. Whereas in the second part, the antimicrobial activity of the P2-functionalized plasmonic paper on both planktonic bacteria and biofilms was tested against two reference strains: Gram-positive Bacteria, i.e., *Staphylococcus aureus* and Gram-negative Bacteria, i.e., *Escherichia coli*, determining microbial inhibition of up to 100% for planktonic bacteria.

Chapter 5 presents the fabrication of SERS-active substrates functionalized by 4-mercaptophenylboronic acid (4-MPBA) to detect bacterial strains such *Escherichia coli* (E. coli) and *Enterococcus faecalis* (E. faecalis). We started deposing three different diameter 500, 607 and 800 nm of polystyrenes (PS) microspheres upon glass slides via convective assembly method. The well-ordered monolayer like crystals as seen by atomic force microscopy (AFM) characterization were then over covered with silver film of 60 nm thickness. Among the three prepared substrates, the selected substrate is represented through this couple dimensions (607 nm, 60 nm) respectively diameter of PS microspheres and film thickness demonstrated by the SEM and AFM images. Subsequently, this chosen substrate has been functionalized with 4-MPBA molecules to discriminate or characterize bacterial strains mentioned above. The analysis of Raman /SERS spectra of *E. faecalis* subtracted from *E. coli* combined with 4-MPBA led to the bacteria identification.

Keywords: Gold nanoparticles, Localized Surface Plasmon Resonance, Biosensors, SERS Spectroscopy, Self-assembling, Antimicrobial Nanoplatform.

CHAPTER 1: PLASMONIC NANOPARTICLES

1.1 History of noble metal nanoparticles

The exact date of gold extraction seems to be ambiguous but according to archeologists, it could be dating to the 3rd or 4th millennium B.C.[1] Thanks to its striking optical properties, gold, in its colloidal forms, has been used in a great number of domains, such texture, architecture and jewelry. Thus, during the days of Roman Empire, artisans had used metal nanoparticles as dyes shown in Figure 1 stained glasses, in cloths and ceramics.[2, 3]

Figure 1. Image of former colloidal particles incorporated in stained glass windows originate from Davos Seaworth. http://guad.deviantart.com/art/Davos-Seaworth-Stained-Glass-Window-330453541

1.2 Optical properties of noble metal nanoparticles

Compared to those observed in the bulk metal, metal nanoparticles (MNPs) possess unique optical properties that vary considerably. When incoming light interacts with MNPs, the electric field of light induces a collective oscillation of the metal surface conduction electrons in resonance. This collective oscillation produces a phenomenon called surface plasmon resonance as SPR [4, 5]. Presenting a variety of shape, size and type of materials, MNPs show different absorption properties corresponding each to a color. In the literature, for instance, colloidal GNPs solution exhibit brilliant colors of diverse range including certain colors when the increasing of size goes from 1 to 100 nm. Moreover, the optical properties of nanomaterial depend on its size and shape. Therefore, all "localized" electromagnetic oscillations (LSPRs) can be involved in SPR. The classical example of LSPR, demonstrated in Figure 2a, arises from the excitation by an external light field of a single spherical gold nanoparticle. Within its absorbance spectrum, as shown illustrated in Figure 2b, only one band of absorption located in the visible region from 500 to 550 nm [6] can be observed.
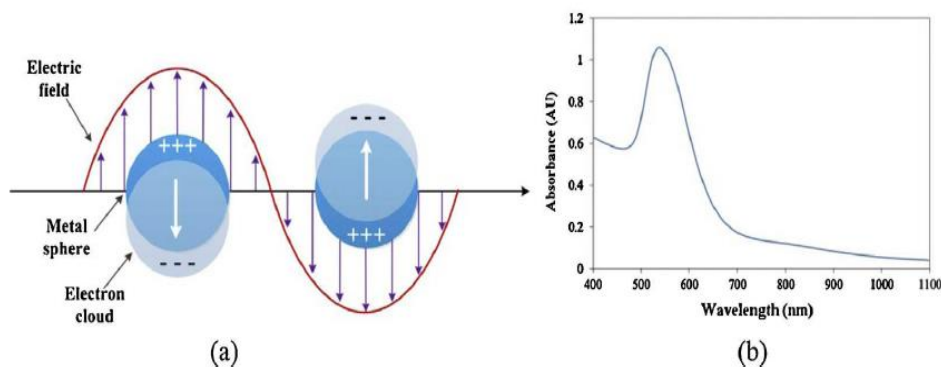
Figure 2. (a) LSPR excitation for AuNSs depicts by an illustration image; **(b)** A representative LSPR absorption band resulting from AuNSs. [7]

For anisotropic nanostructures like GNRs show two LSPR bands as can be seen in Figure 3a and b. One from transversal oscillation and other at higher wavelengths due to the longitudinal oscillation of electron cloud.
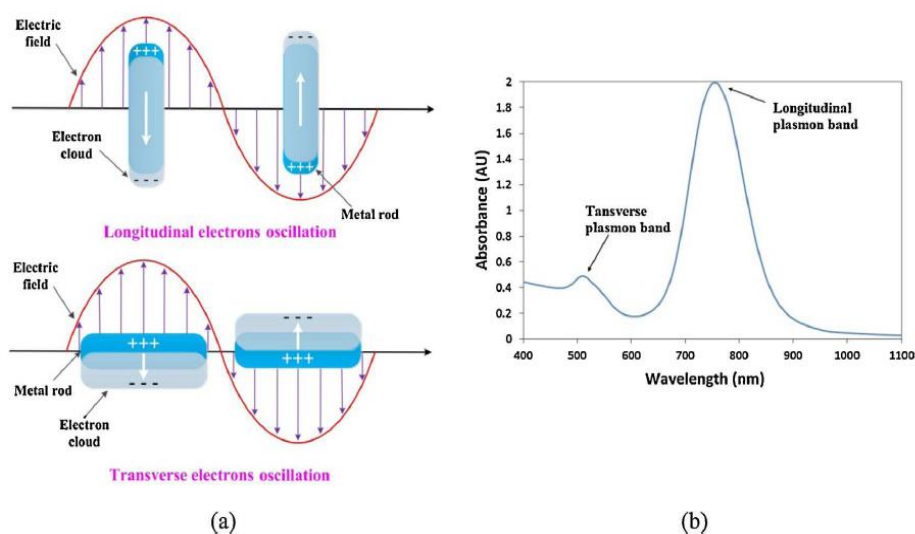
Figure 3. (a) Representative illustration of LSPR excitation for AuNRs and **(b)** The two LSPR absorption bands of AuNRs: at higher wavelengths longitudinal oscillation (Figure 3a top) and transversal oscillation to the short axis (Figure 3a below). [7]

1.3 Gold nanoparticles for biomedical applications

The coupling of biomolecules entities and materials at the nanoscale has the potential to revolutionize many fields of sciences and technology, potentially having a significant impact on current biomedical technologies, nanoelectronics, and related areas [8-16]. Because

nanoparticles and biomolecules typically have the same nanometer length scale, they are natural companions in hybrid systems. Otherwise, modern nanotechnology is inspired partially by biological systems, and it is being developed constantly for new approaches in diagnostics and therapy (theranostics). This why gold nanoparticles (GNPs) are a clear example of their rapid expansion in biomedical applications. Nevertheless, it is well-known that GNPs have been used in medicine for more than 500 years [17], but a truly scientific approach has been applied for studying their biomedical potential only recently [18, 19]. Physicochemical properties and advanced state of synthetic chemistry provide GNPs with an excellent potential for their wide biomedical applications, including diagnostics and therapy of many seemingly incurable diseases. On the other hand, the availability of various gold particles such spheres, rods, cubes, stars, with controlled properties at the nanoscale makes them attractive candidates for the use in biomedical and technological systems. Although GNPs seems to have a good biocompatibility, which goes in favor of their biomedical applications. The advantages of these particles include easy, non-toxic synthesis and chemical modification protocols. Subsequently, the functionalization of nanoparticles due to their binding specificity as well as with large variety of functional groups, biomolecules (nuclei acids, proteins) offer new opportunities to be used in biomedical systems.

CHAPTER 2: FABRICATION METHODS OF SERS SUBSTRATES

2.1. Raman effect

When the light beam is incident on the system of atoms in a molecule, interaction occurs between the electric field of this light and the electron cloud of negatively charged orbitals. This interaction gives rise to the scattering of light by three distinct mechanisms.

(1) In elastic scattering, termed Rayleigh scattering, the frequency of the scattered wave is equal to the frequency of the incident wave $\bar{\upsilon}_0$.

(2) In a form of inelastic scattering, radiation of increasing frequeny is emetted after scattering; this is called anti-Stokes Raman scattering $\bar{\upsilon} = \bar{\upsilon}_0 + \bar{\upsilon}_i$.

(3) In another form of inelastic scattering, radiation of decreased frequency is emetted after scattering; this is called Stokes Raman scattering $\bar{\upsilon} = \bar{\upsilon}_0 - \bar{\upsilon}_i$.

2.2. SERS effect

The typical SERS experiment involves a Raman scattered located at metallic surface or very close to it; these metallic surfaces with electric field enhancement properties are referred to as SERS substrates. One can thus consider that the electromagnetic contribution to the total SERS enhancement is roughly proportional to the fourth power of the field enhancement factor, by assuming that the difference in frequency υ_{Laser}- υ_{Stokes} is small enough to consider a similar enhancement at both the incoming and scattered photons frequency; this implies that the linewidth of the involved plasmon modes, generating the enhancement, is larger than the Raman Stokes shift, which is in most cases true. [20]

2.3. Chemical synthesis of gold nanoparticles

2.3.1. Seed-mediated growth of gold nanorods (AuNRs)

Among the various AuNRs synthesis methods reported, the seed-mediated growth method is the most popular and this has been widely applied due to the simplicity of the experimental procedure, the high yield of nanorods of high quality, the ease of particle size control and the flexibility in structural modifications [21]. The seed-mediated growth approach for colloidal AuNRs was first demonstrated by Jana et al. in 2001. [22]

2.3.2. Seed-mediated growth of gold nanospheres (AuNSs)

This method involves two principal steps to fabricate the gold nanospheres: the first step of this synthesis involved the preparation of Au clusters that were capped by CTAB, these clusters are referred to as the "initial seeds". In this case, aqueous solutions of $HAuCl_4$ and CTAB were mixed at room temperature, followed by the rapid injection of an ice-cold aqueous solution of $NaBH_4$. The resultant brown suspension is directly used as seeds to generate Au nanospheres. In a standard synthesis, aqueous solutions of $HAuCl_4$, CTAC, and ascorbic acid (AA) were mixed at room temperature, followed by the addition of a certain amount of the initial seeds. The mixture turned red within a few seconds, thus indicating the quick formation of Au nanoparticles.[23]

2.4. Self-assembly methods

2.4.1. Convective self-assembly

Such a method is developed by Velev's group [24]. This technique is based on dragging the meniscus at a colloidal solution/ glass substrate/ air interface across the substrate, leaving behind it close-packed arrays of the colloids. Fast deposition times (square centimeters of colloidal crystals in minutes) and control over the number of the layers are some among the many advantages offered by this method.

CHAPTER 3: CONTROLLING END-TO-END ASSEMBLY OF GOLD NANORODS TO ENHANCE THE PLASMONIC RESPONSE IN NEAR-INFRARED

3.1 Experimental details

3.1.1 Chemical synthesis of AuNRs

This method called '' seed-mediated growth solution'' is comprising by two main steps used to produce gold rods through wet chemistry. AuNRs in colloidal of different aspect ratios were synthesized by adapting seed-mediated growth protocol developed by Nikoobakht et al. [25] For the colloidal synthesis of AuNRs with longitudinal LSPR band localized at 738 nm and ~ 3.2 aspect ratio, a typical seed-mediated growth approach was used, involving two-steps [26].

3.2 Characterization of gold nanorods (AuNRs)

3.2.1. UV-vis spectroscopy results

Optical absorption spectrum of the obtained nanoparticles is shown in Figure 4. The plasmonic response presents two LSPR bands one from the transversal oscillations around 519 nm and one at higher wavelengths due to the longitudinal oscillations at 776 nm.
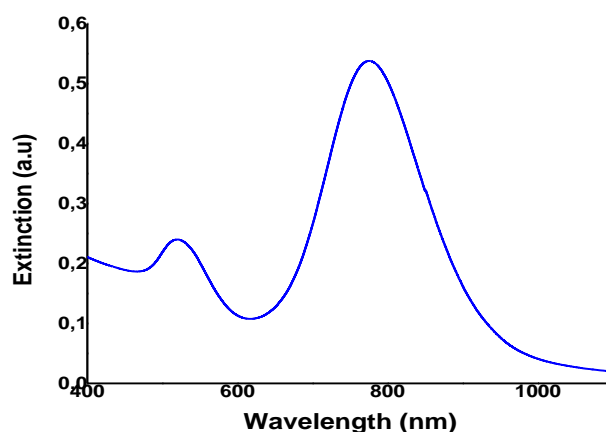
Figure 4. Extinction spectrum of AuNRs.

3.1.2. Transmission electron microscopy (TEM)

The morphology of as synthesized gold nanoparticles (GNPs) was investigated by TEM measurements. Figure 5 shows representative TEM images of synthesized GNPs which clearly proves the synthesis of gold nanorods (AuNRs).
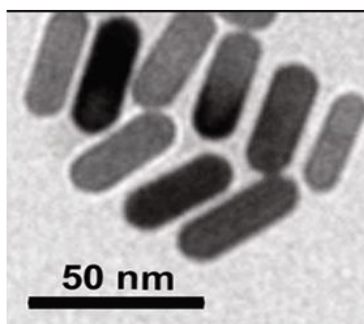
Figure 5. Representative TEM image of AuNRs.

3.3. Results and discussion

3.3.1. Cysteine mediated self-assembly of colloidal AuNRs

First, the pH of the colloidal AuNRs solution was decreased to 3.1 using an aqueous acetic acid solution Figure 6 - blue spectrum, followed by the cysteine molecular linker addition which induced a rapid decrease of the longitudinal LSPR band originally located at 738 nm, whereas a new shoulder at longer wavelength starts to appear Figure 6 – green dashed spectrum. This spectral change is monitored in real-time and associated with the formation of dimers in the first 6 minutes after the incubation Figure 6 – green dashed spectrum, followed with the progressive self-assembling of AuNRs into linear chains after 30 minutes Figure 6 – orange dashed spectrum. This newly formed NIR plasmonic band continues to shift to the red compared with the one recorded after 30 minutes, as a consequence of the further extension in time of the linear assembling reaction of AuNRs in the end-to-end configuration into longer nanochains. To note that, the transversal LSPR band located at 514 nm remains unaffected by the presence of cysteine linker, excluding therefore a possible side-to-side AuNRs assembly. However, the presence of the well-defined isosbestic point at 834 nm is consistent with a "first-order like reaction" between isolated and end-to-end assembled AuNRs as "final products" [27].
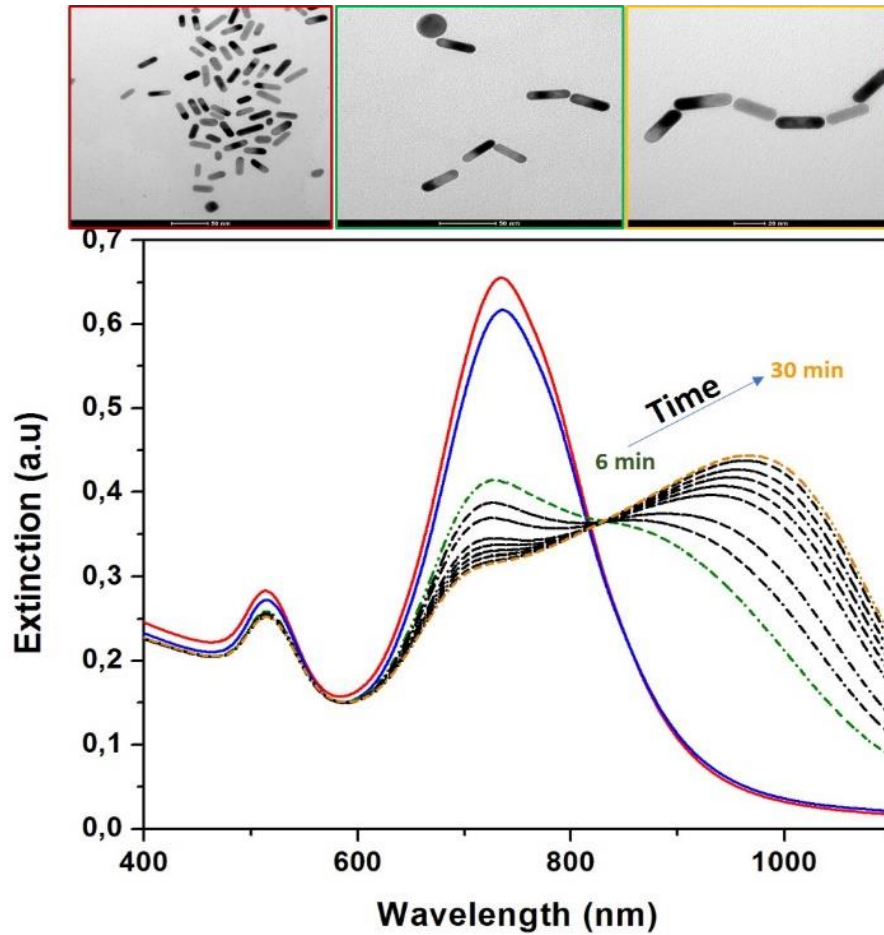
Figure 6. Time-evolution of successively recorded extinction spectra of the end-to-end AuNRs assemblies induced by the Cys linker at pH 3.1 and representative TEM images collected at different assembly process phases (i.e. without Cys linker, after 6 and 30 minutes of incubation with Cys molecules).

3.3.2. FDTD simulations of the end-to-end AuNRs self-assemblies

For a better understanding of the plasmonic properties of the time-depended AuNRs assembling mechanism observed experimentally, we further performed FDTD simulations for three selected cases: i) individual AuNRs with a diameter of 18 and 40 nm length Figure 7A (as obtained from the TEM image), ii) a dimer with a 2 nm gap between the AuNRs Figure 7B and iii) a chain of four assembled AuNRs Figure 7C. Figure 7 shows the comparison of the recorded experimental spectra with the FDTD simulated extinction spectra for the considered types of assemblies, reflecting a good agreement of the obtained data.
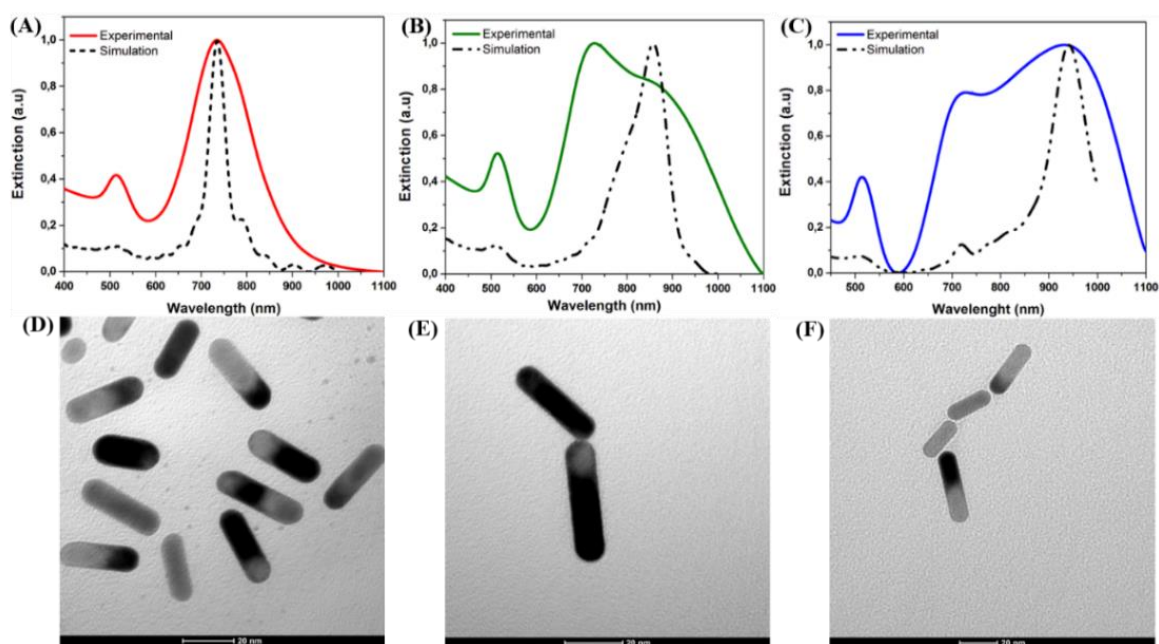
Figure 7. Experimental and FDTD simulated extinction spectra obtained for the considered individual **(A)**, dimers **(B)** and tetramers AuNRs **(C)** end-to-end orientated, and the corresponding collected TEM images during the linear assembling process **(D-F)**. The scale bar is 20 nm.

3.3.3. Amplification of the SERS signal by controlling the end-to-end assembling

It is well known that, when two AuNRs are coupled, a strong electric field is generated in the local nanogap [28, 29]. In this context, the SERS performance of the linear assembled AuNRs compared to individual AuNRs was further investigated by using p-ATP (10^{-4} M) as active Raman reporter and a 785 nm excitation line from a portable Raman spectrometer. In our case, the successful direct grafting of the p-ATP molecules on the individual AuNRs surface was proved by the recorded 16 nm red-shift of the longitudinal LSPR band initially located at 738 nm, without spectral broadening (data not shown). As a first observation, when the p-ATP analyte was covalently grafted onto the tips of the individual AuNRs, the characteristic Raman signal of p-ATP was recorded Figure 8C.

In contrast, when the p-ATP-grafted AuNRs in aqueous solution start to self-assemble via the Cys linker, the spectral behavior of the end-to-end linear assembly is observed, together with a considerably enhanced Raman signal of the p-ATP molecules localized at the junctions of the AuNRs Figure 8D. This effect is ascribed from the generated hot spot regions of the AuNRs

assemblies, proving therefore that the linear AuNRs chains give arise to a much stronger SERS signal compared to the individual AuNRs.

Subsequently, in order to understand the modification of the Raman intensity of the p-ATP analyte molecule in the two above investigated cases, we also evaluated -by employing the FDTD method- the distribution of the relative electromagnetic field intensity $|E/E_0^2|$ at the surface of an individual AuNR Figure 8A and six assembled AuNRs in an end-to-end manner Figure 8B.
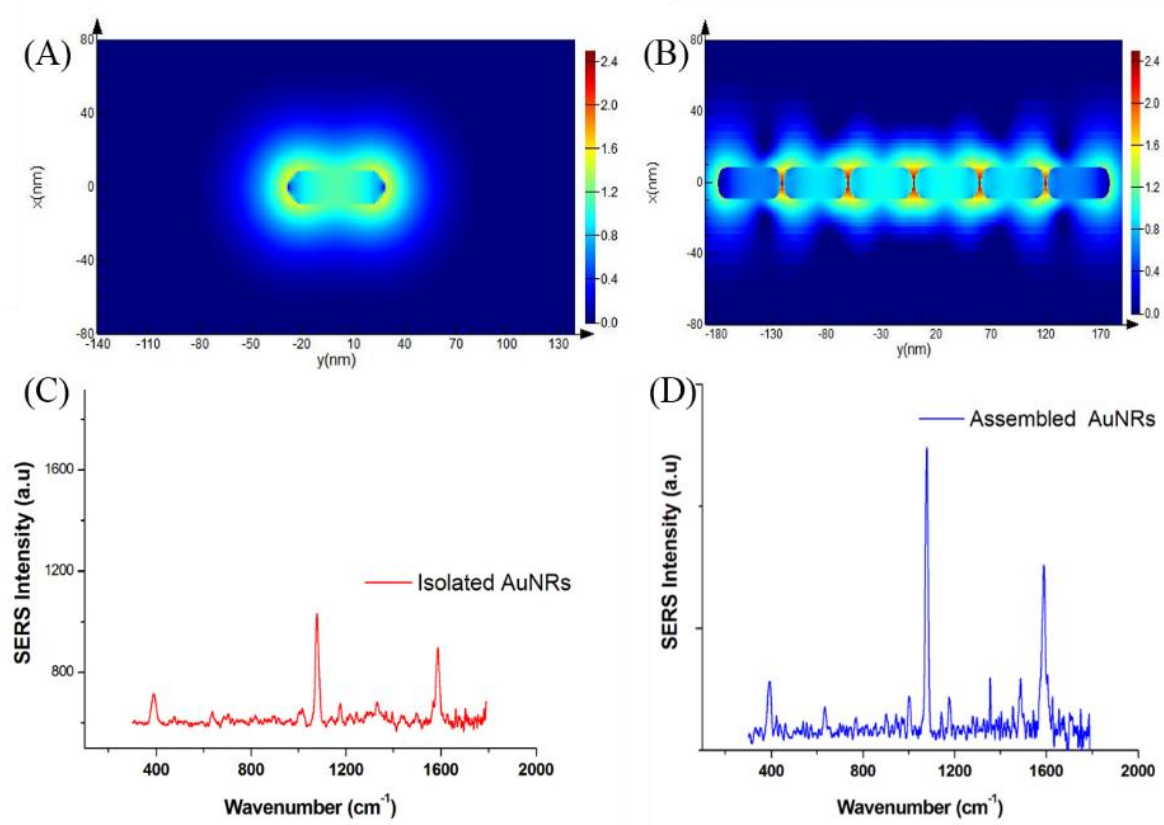
Figure 8. Calculated $|E/E_0^2|$ maps for an individual AuNR with the length of 40 nm and diameter of 18 nm **(A)** and 6 perfectly assembled AuNRs linear chain **(B)** under 785 nm laser excitation, obtained by employing the FDTD simulations; SERS spectra of p-ATP grafted on isolated AuNRs **(C)** and linearly assembled AuNRs **(D)**, using a 785 nm laser excitation.

CHAPTER 4: VERSATILE POLYPEPTIDE-FUNCTIONALIZED PLASMONIC AS SYNERGISTIC PAPER BIOCOMPATIBLE AND ANTIMICROBIAL NANOPLATFORM

4.1. Experimental details

4.1.1. Colloidal gold nanospheres synthesis

For the fabrication of the CTAC-stabilized gold nanospheres (AuNSs), an adapted version of the successive seed-mediated growth approach previously reported by Zheng et al. [30] was employed

4.1.2. Optical and morphological characterization of AuNSs before and after their immobilization onto the paper substrate.

In this context, the optical response of the as-synthesized nanostructures was recorded using an UV-Vis-NIR spectrophotometer. In Figure 9, the blue spectrum corresponds to the AuNSs in aqueous solution, as expected, they exhibit one LSPR band at 529 nm due to the oscillations of the conduction electrons at the surface of the nanostructures, a phenomenon theoretically described by the Mie theory [31]. The upper-right inset shows a representative TEM image of the as-synthesized AuNSs, thus confirming their spherical shape.
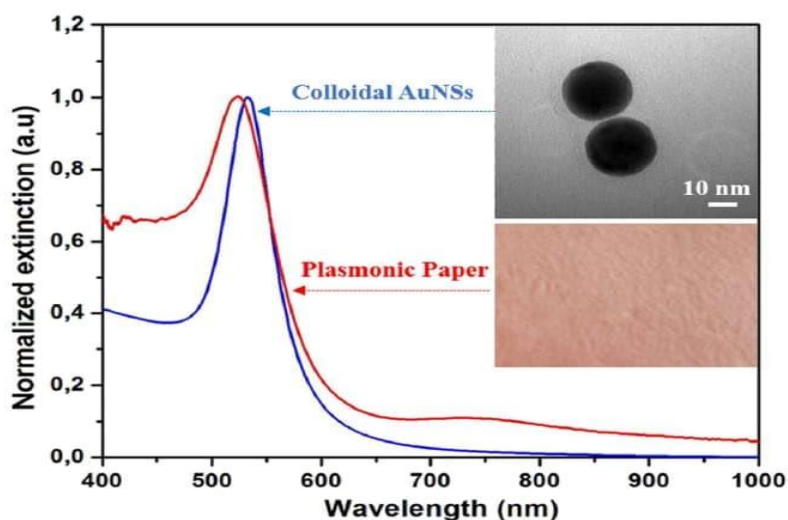
Figure 9. The normalized extinction spectra of the AuNSs before and after their immobilization onto the paper substrate. Inset upper-right: A representative TEM image of the as-synthesized AuNSs. Inset lower-right: A digital photograph of the paper substrate after the immobilization of the AuNSs.

Additionally, the surface potential was investigated by zeta potential measurements revealing the positive value of + 51 mV. This particular feature is highly advantageous for the further adsorption of the nanostructures. In fact, the uniform adsorption of the AuNSs onto the paper fibers is due possibly to the electrostatic interaction between the positively charged nanoparticles and paper, which presents a large number of hydroxyl groups that are accessible, in general, for attaching positively charged species [32,33]. Subsequently, the LSPR response of the plasmonic paper was recorded (Figure 9: red spectrum), the optical response of the colloidal nanostructures is well-preserved, indicating the immobilization of individual nanospheres on the cellulose fibers without large scale aggregation. Moreover, the extinction band underwent a blue-shift of 5 nm, which is not surprising given that the LSPR is highly sensitive to the surrounding environment of the nanoparticles, and hence it depends on the refractive index of the medium they are in. By drying the plasmonic paper, the AuNSs are transferred from water (n = 1.333) and placed in air (n = 1). All of these results confirm the successful immobilization of the AuNSs onto the paper substrate. Furthermore, the SEM analysis of the plasmonic paper consolidates the obtained optical results. Figure 10a and b present representative SEM images of the cellulose fibers before and after the AuNSs immobilization onto the cellulosic fibers (as white dots), respectively.
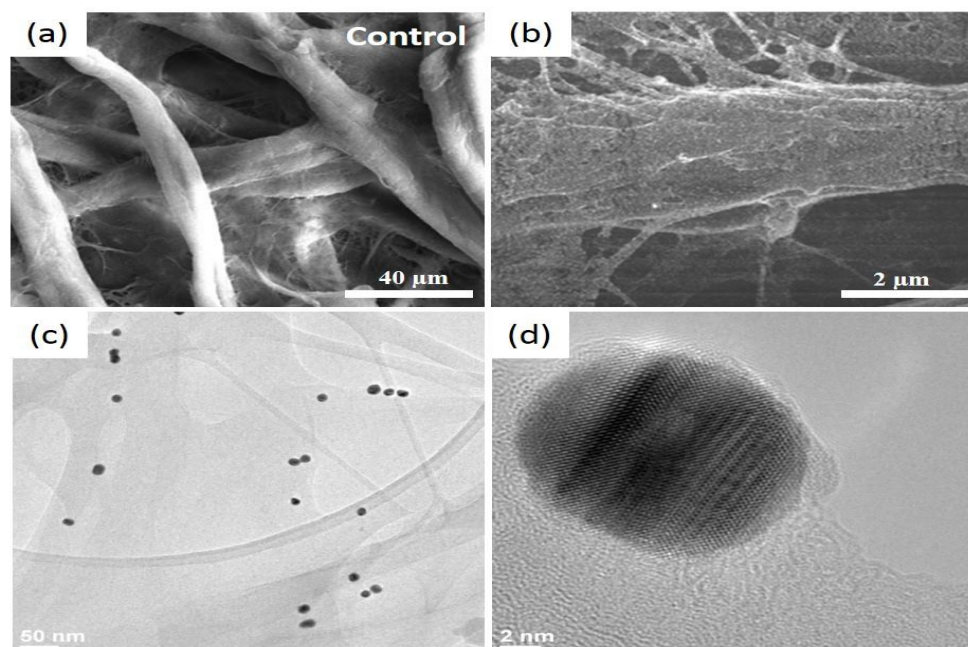
Figure 10. Representative SEM images of the pristine Whatman paper presenting its interconnected microfibers **(a)** and after the uniform decoration of the paper surface with the AuNSs (bright spots) **(b)**, as well as typical HRTEM images at low **(c)** and at high resolution **(d)**.

The AuNSs are well-adsorbed on the 3D porous structure of the Whatman paper, thanks to the electrostatic interaction between the two opposite surface charges. Additionally, they present a homogenous distribution like a thin film, without large scale aggregation. For a higher magnification, HRTEM was employed to distinguish the individual nanostructures (Figure 10c) by wetting the paper with alcohol and scratching it to obtain a debris, which was then dropped onto a carbon grid and left to dry prior to the analysis. The HRTEM-obtained results are in good agreement with the optical determinations and concluding that, after the immobilization, the AuNSs maintained their shape and size; the heat drying treatment, nor the successive immersion steps, did not induce any morphological changes. Zooming in even further, the crystallinity of the AuNSs can be assessed as single-crystal nanospheres (Figure 10d).

After the adsorption of the AuNSs onto the paper matrix, the nanoplatform's functionalization with the P2 polypeptide was further addressed. Considering the amino groups' affinity to bind to the gold surface, the P2 was grafted by dropping 10 μL aqueous solution of 50 μM of P2 molecules to create a polypeptide monolayer on the plasmonic paper. After the functionalization with P2, the extinction band of the plasmonic paper records a 7 nm red-shift indicating that the micro-environment in the close vicinity of the AuNSs has changed again, thus confirming the successful functionalization with the P2 polypeptide (Figure 11a). Moreover, steady-state fluorescence technique was next employed to obtain valuable information regarding the electrostatic interaction between P2 peptides and AuNSs' surface (Figure 11b), by monitoring the strong fluorescence emission of the P2-functionalized plasmonic paper (Figure 11b: green spectrum), compared to the free P2 molecules dropped onto Whatman paper (Figure 11b: black spectrum), within the spectral region between 295 and 500 nm, employing a fixed excitation wavelength at 280 nm. As we can see in Figure 11b: black spectrum, the P2 polypeptides grafted directly onto the Whatman paper exhibits a strong intrinsic fluorescence emission band at 339 nm, which originates from the emission of the Tryptophan residues. Tryptophan residues are, in general, highly sensitive to changes of the local environment, and, therefore, when the P2 molecules were grafted onto the plasmonic paper, a red-shift of the fluorescence emission up to 9 nm, from 339 to 348 nm, was noticed, indicating polarity changes around the tryptophan residues, which corroborate results obtained from the LSPR spectra, leading to the conclusion that the P2 polypeptide was successfully bound to the AuNSs adsorbed onto the paper substrate.
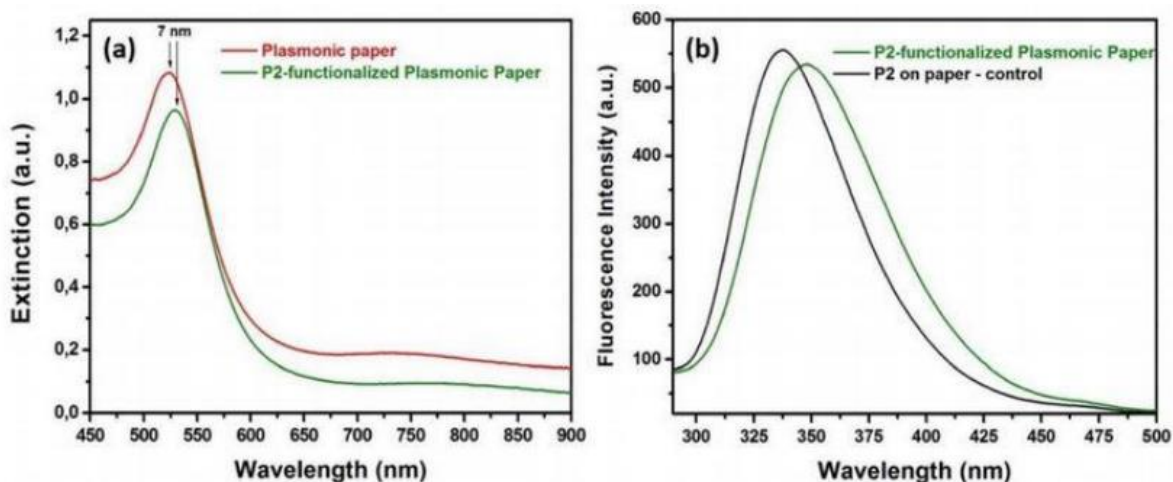
Figure 11. (a) The extinction spectra of the plasmonic paper before and after the functionalization with the P2 polypeptide and **(b)** fluorescence spectra of P2 on bare paper and on the designed plasmonic paper substrate.

4.2. Fabrication and functionalization of the plasmonic paper support

In order to fabricate the plasmonic paper substrate, Whatman no.1 filter paper was employed, from which paper strips were cut. For the immobilization of the nanoparticles, the strips were then immersed in the colloidal solution and left to soak for 10 min. The substrates were dried at 45 °C for an additional 10 min. To ensure a high loading of AuNSs on the paper fibers, the immobilized nanoparticle concentration was increased by the application of the immersion procedure for 3 consecutive times. The plasmonic paper was then functionalized with synthetic P2 polypeptide, by dropping 10 μL aqueous solution of 50 μM of P2 molecules to create a polypeptide monolayer on the plasmonic paper.

4.2.1. The biocompatibility of the functionalized plasmonic paper

Compared to the control BJ cells, the cells grown in the presence of P2 or the paper alone present a slightly increased viability, thus demonstrating that the two components are not toxic for the skin cells, as expected. Previous studies have reported that, paper-based platforms, like the Whatman paper, are gaining ground in biomedical applications due to their biocompatibility with eukaryotic cells, cost efficiency, accessibility, etc. [34]. Moreover, these results are in good agreement with a previous study on the P2 polypeptide, which assessed that P2 has no toxicity against eukaryotic cells at the concentrations used herein [35].
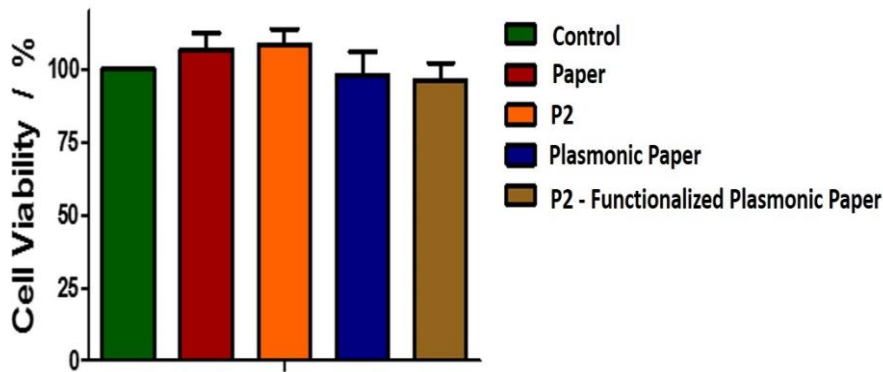
Figure 12. Biocompatibility of the new nanoplatforms against human BJ cells.

However, in the presence of the plasmonic paper and P2-functionalized plasmonic substrates, a small decrease in cell viability is observed. After the incubation with both plasmonic systems, the viability decreases 10%. Nonetheless, the decrease is not significant, indicating that the new obtained plasmonic nanoplatforms are not toxic for human skin cells, favoring their further implementation in antibacterial applications.

4.2.2. Evaluation of the BJ cells morphology and viability by in vitro Fluorescence Imaging

Further, we investigated the structural changes induced in the BJ cells by the plasmonic nanoplatforms.

Figure 13 presents representative confocal fluorescence microscopy images of the BJ cells in all tested conditions after the staining process of the nucleus with Hoechst 33,342 (blue) and actin filaments with Phalloidin-FITC (green). The control cells have an elongated, bipolar morphology, with actin filaments well-organized, almost parallel, going almost from one end to the other end of the cell Figure 13A. Additionally, the nucleus shows with its specific ovoid morphology. Similar characteristics are observed for the cells grown in the presence of the Whatman paper Figure 13B and peptide P2 Figure 13C, thus confirming, along with the viability tests, that alone the two do not induce any changes in the cell structure. In the cases of the plasmonic paper-based nanoplatform without Figure 13D and functionalized with the antimicrobial peptide P2 Figure 13E, some morphological changes are observed. Instead of the specific elongated shape, the BJ cells show an altered shape becoming smaller with a stellar morphology, with 3 or more processes extending from the cell body. Also, the actin filaments are less organized as compared with the control cells. Even though, the shape of the cells has

changed, the nucleus doesn't show any modifications, indicating that the cellular functions are not affected. This observation is sustained also by the fact that the cells were found in division in both cases.
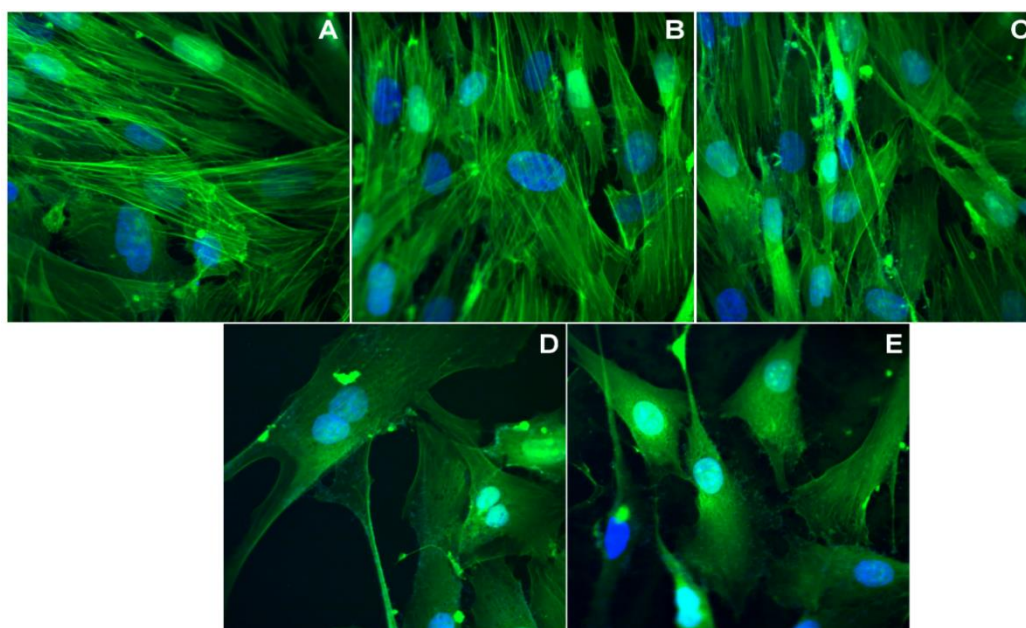
Figure 13. Confocal fluorescence microscopy images emphasizing the structural changes of the BJ cells after the 24 h treatment with: **(A)** no treatment-control cells, **(B)** Whatman paper itself, **(C)** free P2, **(D)** plasmonic paper-based nanoplatform and **(E)** P2-functionalized plasmonic nanoplatform. Scale bar is 10 μm.

Anew, the obtained results are well correlated with the reported for MTT viability assay, the number of grown cells is decreased in the presence of the plasmonic nanoplatforms despite showing cell division functionality.

To conclude, the developed plasmonic nanoplatforms were demonstrated to be biocompatible for the human skin cells using two complementary techniques, thus supporting their further testing in terms of antimicrobial activity.

4.2.3. Antimicrobial activity on planktonic and bacterial biofilms

Further, the microbial activity of our plasmonic paper-based nanoplatform was tested in two different cases: (i) planktonic bacteria: generally described as independent, untethered planktonic cells in diluted suspensions, and (ii) bacterial biofilms: formed by the adhesion of the bacterial cells to each other or to a surface. For both situations, the Gram-positive

Staphylococcus aureus 12600 and Gram-negative *Escherichia coli* 25922 strains were chosen for the validation and evaluation of the antimicrobial effect of the proposed plasmonic paper-based nanoplatform. In the case of the planktonic bacterial, the plasmonic paper was investigated in two configurations, specifically in the absence and functionalized with the chemically synthesized P2 polypeptide. As control, we followed the same experimental procedure without the plasmonic paper.

Firstly, the classical dilution-extraction colony-counting method was employed. The plasmonic paper with and without P2 showed strong antimicrobial activity, as supported by their capacity to reduce the bacterial growth with more than 6 logCFU/mL. The residual antimicrobial activity of the discs combinations after extraction was absent, as checked by the disc diffusion method both towards *S. aureus* and *E. coli*. However, it seems that though the antimicrobial components are extractible, they are not as equally diffusible, because non-extracted discs did not develop large inhibition diameters Table 1. An inhibition zone of 5 mm indicates the absence of an antimicrobial diffusible effective substance, as the 5 mm are represented by the disc diameter itself.

Table 1. Comparative antimicrobial activity of the different disc combinations before and after extraction of antimicrobial active components expressed by the diameter of inhibition.

Disc/Peptide	*Staphylococcus aureus* 12600		*Escherichia coli* 25922	
	Before Extraction	After Extraction	Before Extraction	After Extraction
Blank/P2 50 mM	5 mm	5 mm	5 mm	5 mm
Plasmonic Paper/0	6 mm	5 mm	6 mm	5 mm
Plasmonic Paper/P2 50 mM	6 mm	5 mm	6 mm	5 mm

Further, the differential antimicrobial activity of our designed plasmonic nanoplatform, as documented in the second, more sensitive colony counting experiment, can be visually confirmed by observing the colony counting plates as seen in Figure 14a, b, in the presence of the P2-functionalized plasmonic paper the bacterial growth is drastically reduced. To assess the capability of each paper-based nanoplatform to efficiently inhibit the bacterial growth, the number of colony forming units (CFU/mL) was determined and further expressed as percentual inhibition rates Figure 14. For instance, the plasmonic paper alone inflicts a growth reduction of 23% (6 logCFU/mL) of the *Staphylococcus aureus* 12600 bacteria, however, its anti-bacterial

activity is much more efficient for *Escherichia coli* 25922, leading to a 63% (6.6 logCFU/mL) inhibition rate. After the functionalization of the plasmonic paper with the P2 polypeptide, the bacterial colony formation is totally inhibited, the growth reduction rate being significantly improved by reaching for both Gram-positive and Gram-negative strains 100% (7 logCFU/mL).
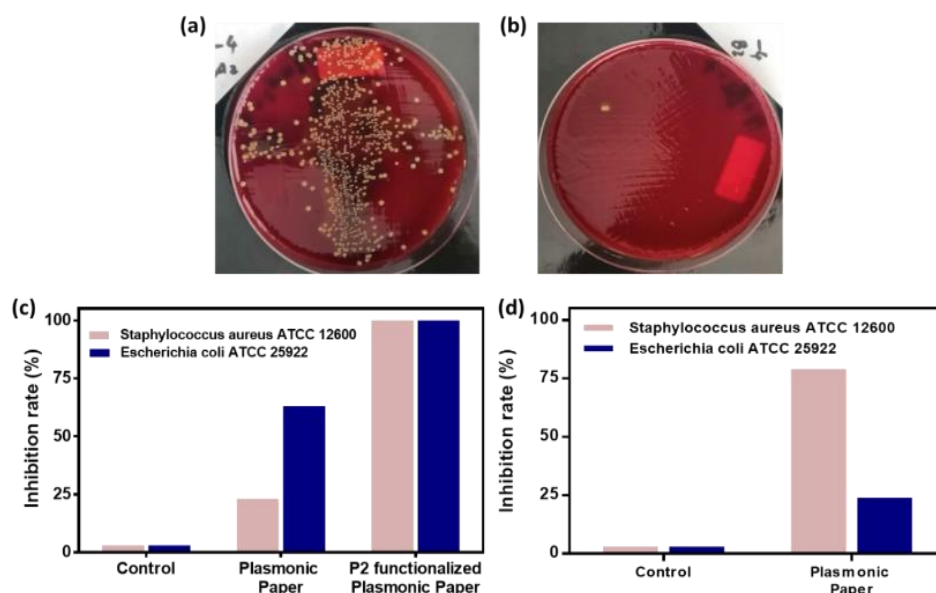
Figure 14. Representative digital images of the colony counting plates with *Staphylococcus aureus ATCC 12600* showing the anti-microbial activity against planktonic bacteria without **(a)** and with the P2-functionalized plasmonic paper **(b)**; The bacterial growth inhibition rates for **(c)** planktonic bacteria and **(d)** bacterial biofilm determined for the as-designed paper-based nanoplatform when applied to both *Staphylococcus aureus ATCC 12600* and *Escherichia coli ATCC 25922* bacterial cultures.

Furthermore, the bacterial growth inhibition was tested for the plasmonic paper during the biofilm formation of both bacterial strains. As expected, the control samples exhibit 0% inhibition, as their growth process is not altered or disturbed in any way. Compared to the antimicrobial activity against planktonic bacteria, for bacterial biofilm growth inhibition the plasmonic paper is 3.3-fold more efficient against *Staphylococcus aureus* ATCC 12600 reaching a 79% growth reduction rate compared to 24% against *Escherichia coli* ATCC 25922.

CHAPTER 5: FABRICATION OF SERS SUBSTRATES BY CONVECTIVE ASSEMBLY OF POLYSTYRENE MICROSPHERES

5.1. Experimental details

5.1.1. Convective assembly

Convective self-assembly is developed by Velev's group [36]. This technique is based on dragging the meniscus at a colloidal solution / glass substrate / air interface across the substrate, leaving behind it close-packed arrays of the colloids. Fast deposition times (square centimeters of colloidal crystals in minutes) and control over the number of the layers are some among the many advantages offered by this method see Figure 15. Three different diameters of polystyrenes (PS) were used in our study 500, 607 and 800 nm.
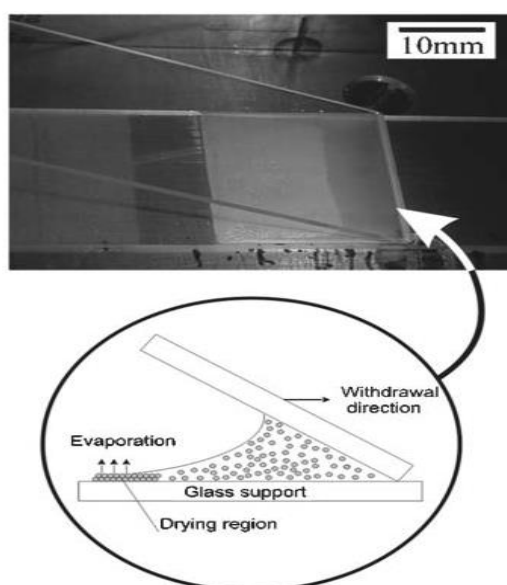
Figure 15. Schematic of the experimental setup for colloidal crystal assembly [37].

5.2. Optical and morphological characterizations of Glass substrates

5.2.1. UV-vis spectroscopy results

As illustrated on Figure 16, the as–fabricated substrates were thoroughly characterized optically. The most striking feature in the reflectivity spectra is the presence of the first order waveguide mode also called "first –order mode or resonance". As can be seen on Figure 16 by the arrows, they are located at around 600, 720 and 980 nm respectively for 500 (red spectrum),

607 (yellow spectrum) and 800 nm (pink spectrum) diameters. Therefore, the reflectance of these polystyrene microspheres exhibits different plasmonic responses.
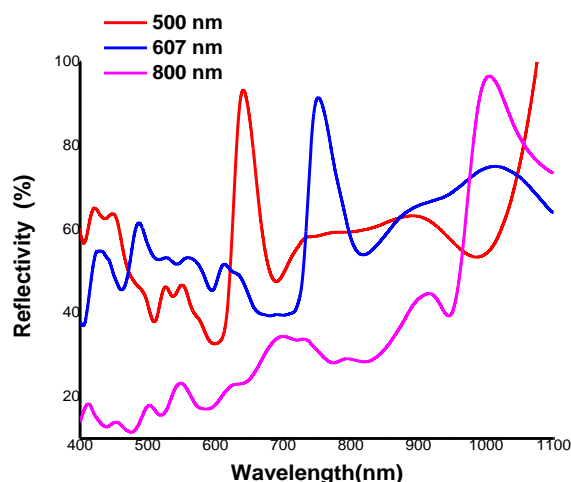
Figure 16. Reflectivity optical spectra of PS 500, 607, 800 nm colloidal monolayer crystals.

5.2.2. Atomic force microscopy (AFM)

The AFM images with higher magnification in Figure 17 display clear evidence that the monolayer exhibits a close packed hexagonal ordered arrangement of polystyrene spheres PS. Additionally, the images show that the monolayer PS arrays exhibit hexagonal packing on the substrate over a large area, which contribute to the formation of high-quality ordered array of PS. Also, Figure 17 shows AFM images of PS spheres monolayer colloidal crystals fabricated at different volume and deposition speed.
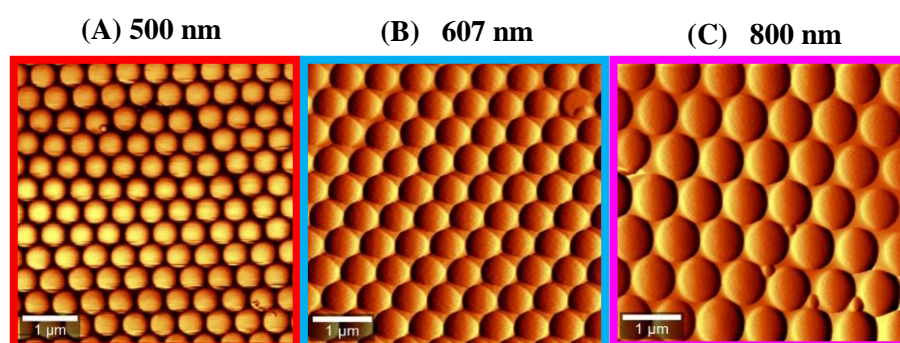
Figure 17. AFM images monolayer PS colloidal-crystal prepared using different diameter (scale bar 1 μm): **(A)** 500 nm; **(B)** 607 nm; **(C)** 800 nm.

5.3 AFM and SEM characterization silver films deposited on colloidal crystal monolayer

The deposition of the Ag film used as SERS substrate was performed using a lab-10 molecular-beam epitaxy (MBE) system. In order to reach our goal, 60 nm Ag film was deposited over polystyrene surface meaning over 500, 607 and 800 nm.

5.3.1. Atomic force microscopy (AFM)

The resulting metal/dielectric nanostructures were characterized by AFM method after depositing 60 nm Ag films. Further, AFM images in Figure 18 (top row) show distinctive local zones produced by the presence of silver particles at the surface of the material which contrasts with the reference sample that consists of pure PS. This is an indication that the top of the polystyrenes is covered by silver particles which can interact differently with the crystals surface.

Based on top–view in Figure 18(bottom row), the AFM phase images revealed the presence of low roughness on top of the nanocrystals surface.
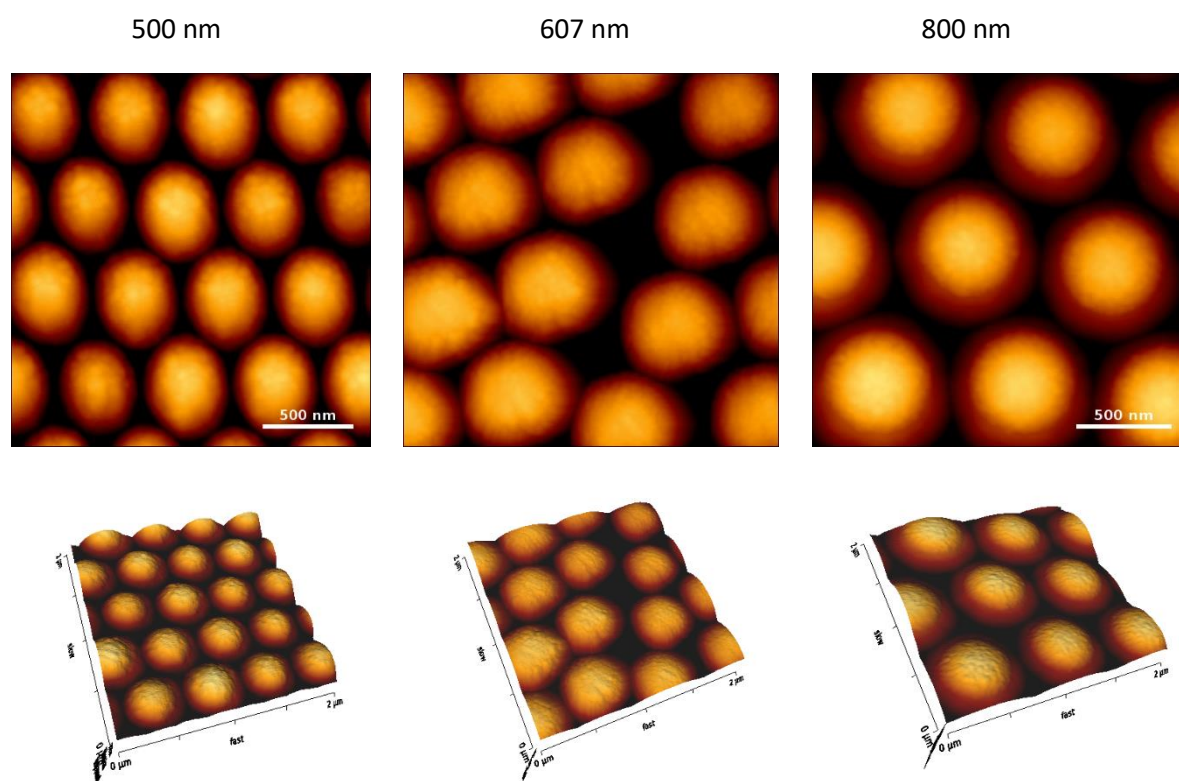
Figure 18. AFM images of silver coated 60 nm thickness colloidal crystals monolayers made of PS spheres of 500, 607 and 800 nm.

5.3.2. Scanning electron microscopy (SEM)

As demonstrated by SEM images in Figure 19, shows corrugation, nanometer-sized gaps, sharp apexes, or ridges on top of the colloidal crystals which can hypothesize SERS-hot-spots presence. Because strongly enhanced fields and giant SERS enhancement factors are further promoted by the presence of nanoscale roughness such as edges, apexes, corners, or gaps on the metallic nanostructure surface. [38, 39] Our case revealed the presence of certain inorganic compounds on top of the formed-nanocrystals surface. Moreover, as can also be observed in the SEM images, the colloid crystals are not decoupled, a bridge is formed, and that interconnects each sphere to its neighbors. Alongside this, there is brightness even though this brightness over the surface can be attributed to the negligible role of film surface roughness for the SERS enhancement. Meanwhile, AFM image in the case of 607 nm diameter suggests that highly enhanced electromagnetic (EM) fields are localized around the rims and at the junctions between nanocrystals but always in between neighboring silver-coated polystyrene spheres. As the nanocrystals are here in close contact as shown AFM image in 607 nm diameter case, the local electromagnetic fields are expected in between the silver- coated microspheres.
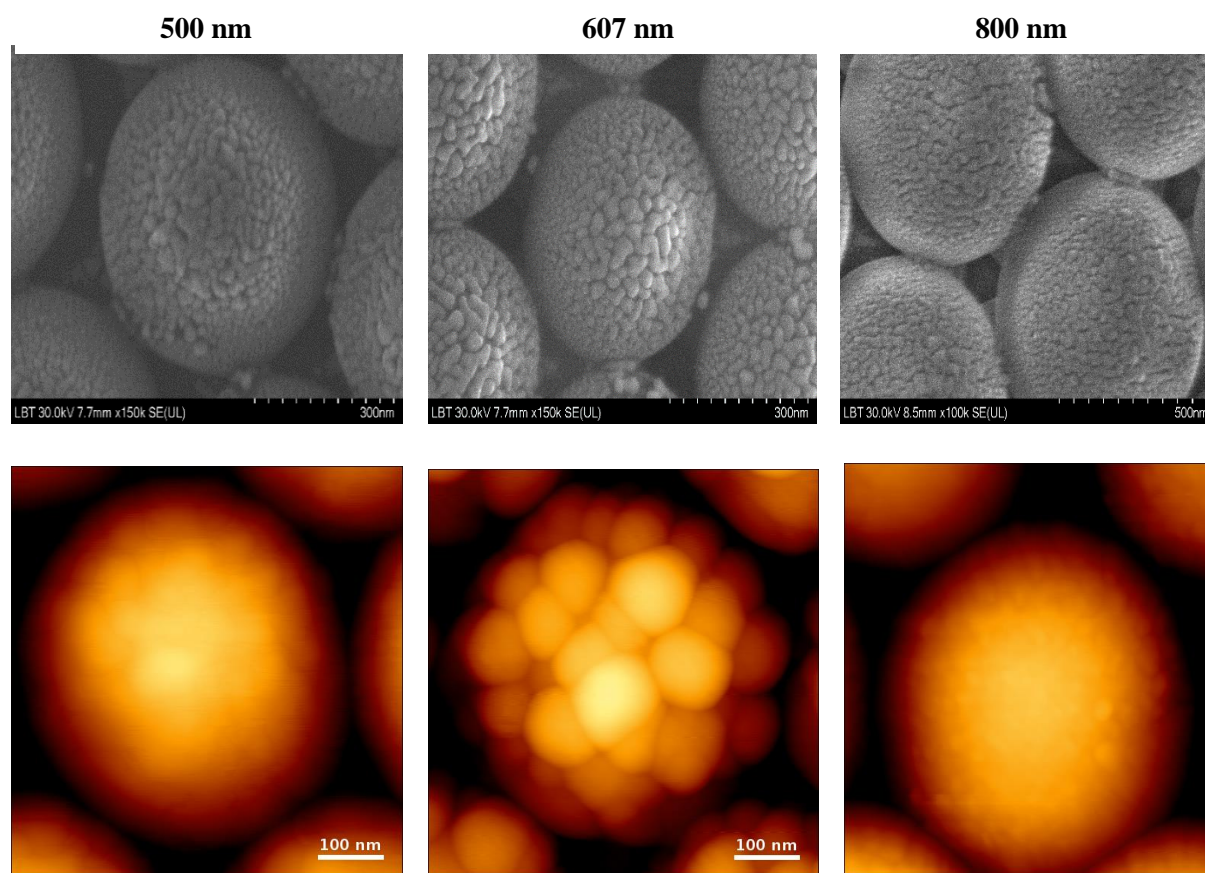
Figure 19. SEM and AFM images of silver 60 nm thickness coated colloidal crystals of 500, 607, and 800 nm diameters.

As shown Figure 19, Scanning electron microscopy (SEM) and atomic force microscopy (AFM) images made show the roughness of surface at the top of the different diameters of PS 500, 607 and 800 nm. Based on all these striking observation and remarks pointed up in this work, we have decided to continue the following steps of this study by focusing on nanocrystals made by 607 nm microspheres coated with 60 nm Ag film.

500 nm   **607 nm**   **800 nm**
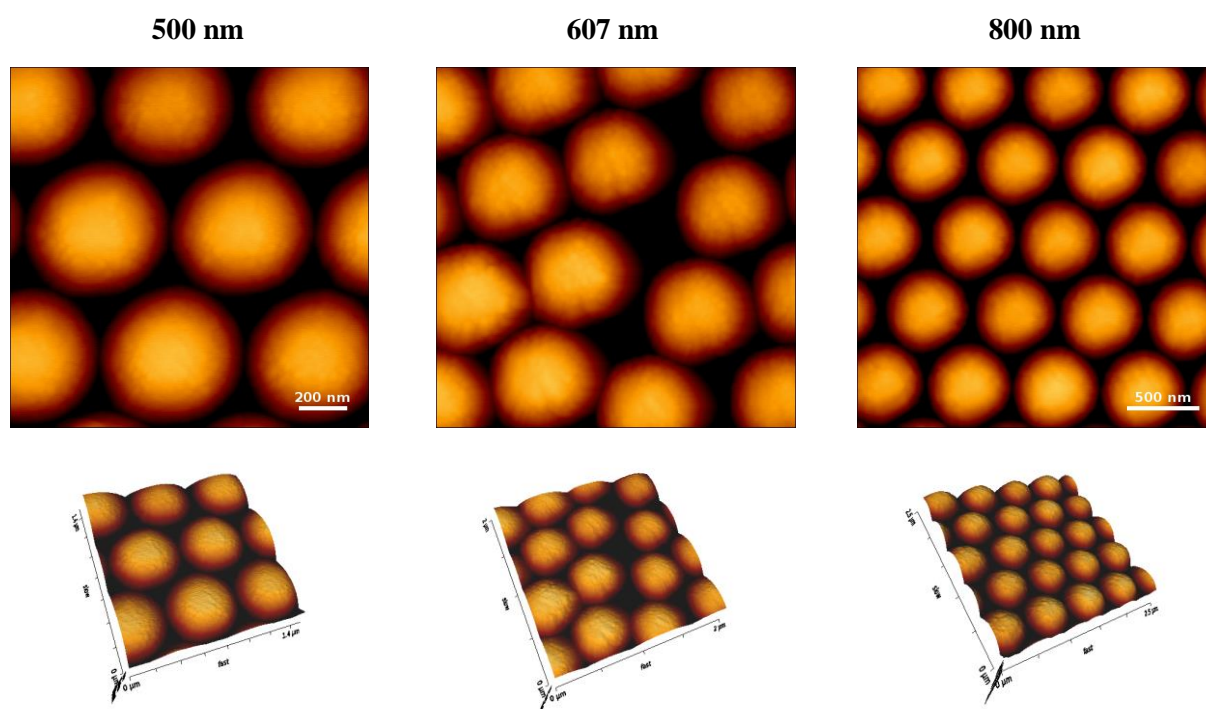
Figure 20. AFM images of silver coated (30, 60 and 90 nm thicknesses) colloidal crystals monolayers made of PS spheres 607 nm diameter.

Actually, SERS substrates fabricated by a thin metal layer onto self-assembled colloidal crystals stipulate that the plasmonic and SERS properties of such substrates are determined by the size of the colloidal templates used and the thickness of the deposited metal film.

5.4 Assessment of SERS-activity and detection of Escherichia Coli and Enterococcus faecalis

With this aim, we tested several SERS-active substrates for detection of two representative bacteria species, namely Gram-negative *Escherichia coli* (*E. coli*) and Gram-positive *Enterococcus faecalis* (*E. faecalis*) respectively. For this aim, the molecule 4-MPBA molecules were adsorbed upon these three substrates coated with 60 nm Ag film (500, 607 and 800 nm diameter of polystyrene microspheres). Figure 21 shows the reproducibility of SERS spectra of

E. coli and E. *faecalis* respectively. All recorded spectra were normalized in accordance with the intensity of the most intense band after subtracting the baseline. In order to demonstrate the spot-to-spot reproducibility, several spectra were acquired from various locations on the same sample. This space between individual silver nanocaps coating may be between 50 and 150 nm, which is much smaller than that of a bacterium (micrometer scale), thereby ensuring that the captured bacteria would lie flat on the surface [40]. It is known that the roughness of metallic surface can dramatically enhances the Raman scattering of analytes adsorbed on the surface [41,42]. Therefore, we concluded that SERS activity of our substrates is mainly sustained by the electromagnetic hot spots located at the inhomogeneous arrangement of silver particles as well between the metallic nanocaps on the top of regular microsphere arrays.
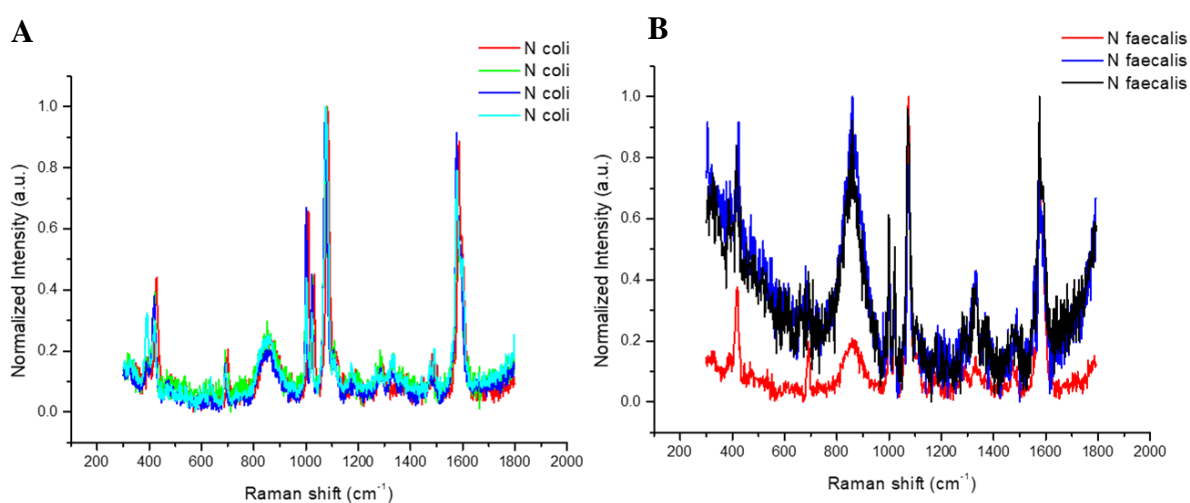
Figure 21. Reproducibility of SERS spectra of *E. coli* (**A**) and *E. faecalis* (**B**) collected from different spots on the substrate.

We have chosen for detection as proof-of concept, two representative bacteria species, Gram-negative *Escherichia coli* (*E. coli*) and Gram-positive *Enterococcus faecalis* (*E. faecalis*) respectively. This SERS activity was firstly evaluated through the detection of 4-MPBA as bio-recognition molecules and Raman reporter. The boronic acid group from 4-MPBA will bind to peptidoglycan from the cell wall of the bacteria [43]. In the SERS detection step, 4-MPBA acting as Raman reporter molecule provide a strong Raman signal. Currently, the Raman fingerprints of 4-MPBA show corresponding to changes when bacteria are deposited on the substrate. This can be used to discriminate different kinds of bacteria. Further, we investigated the efficiency of our biosensor by comparing the SERS spectra of both bacteria in presence of 4-MPBA molecule. This SERS spectrum represents a superposition of the molecular vibrations of specific cellular compounds [44].

Figure 22A depicts composite of SERS spectra collected from those substrates cultivated with two bacterial species (Gram-negative *E. coli* and Gram-positive *E. faecalis*) together with the reference spectrum collected from the substrate functionalized with 4-MPBA biomolecules. It is trustworthy to notice that the components and architecture of bacterial envelope are very different between gram-positive and gram-negative bacteria. [45]

We can notice by naked eyes that both bacteria exhibit almost identical spectra, otherwise, the Raman bands of 4-MPBA are present among the composite of SERS spectra collected from two bacteria. There are still minor differences between the two strains in the peaks ranging from 1100 to 1700 cm^{-1} as can be seen in Figure 22B, a zoom- in view shows this broad band at 1602 cm^{-1} and these three peaks at wavenumbers 1198, 1482, and 1502 cm^{-1} [46-50] were observed in the spectrum of *E. coli*. Moreover, only one band at 1602 cm^{-1} (C=C), phenylalanine vibration ring which belongs to *E. coli* [51-53]. Due to the appearance of this band, we can confirm the presence of *E. coli*. While one unique band at 1332 cm^{-1} assigned to -C-stretch of phenyl is specially provide by *E. faecalis*. Consequently, we remarked that band arising from 4-MPBA do not interfere with the representative bacterial fingerprint bands in the range between 1100 and 1700 cm^{-1}. However, a specific statistical analysis is on progress to disentangle such minor differences between the SERS spectra.
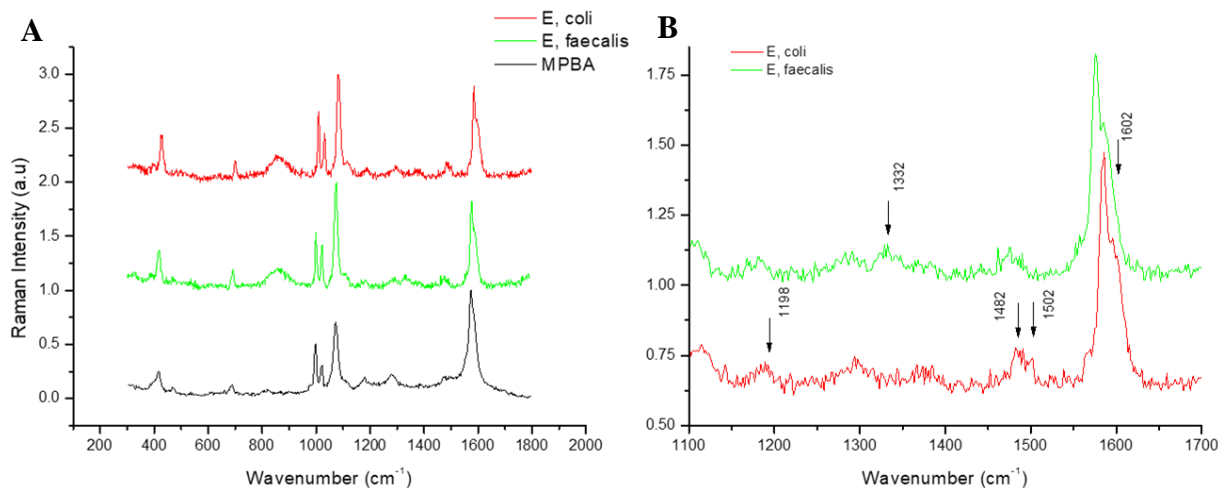
Figure 22. (A) Normal Raman signal of *Escherichia coli* (*E. coli*), *Enterococcus faecalis* (*E. faecalis*) and 4-mercaptophenylboronic acid (4-MPBA); **(B)** Specific peaks of *E. coli* and *E. faecalis*.

FINAL CONCLUSIONS AND FUTURE WORK

➤ We were successfully able to synthesize highly reproducible AuNRs via the seed-mediated growth approach. The process of the self-assembling was initiated by changing the pH to more acidic at 3.1 and then added the cysteine (Cys) molecule and monitored in real-time for minutes up to hour the transmission electron microscopy (TEM) images presented long AuNRs chains corresponding to more intense NIR (near-infrared) plasmonic response. Moreover, the presence of the isosbestic point observed at 834 nm suggests the presence of both isolated and assembled AuNRs.

➤ Subsequently, we compared our experimental results with numerical simulations of the systems by performing Finite-difference time-domain (FDTD) simulations. And we realized that the theoretical FDTD results overlap with the experimentally obtained plasmonic results.

➤ Additionally, the electric fields in the hot spots in between the linked nanoparticles was proved by SERS experiments using as target analyte para-aminothiophenol (p-ATP) and conducted to clear demonstration of a higher enhancement factor relative to the individual AuNRs.

Future work could involve evolution study of the coupling in time and localize SERS signal in the chain during the evolution time.

➤ We synergistically combined the advantage of the positively-charged gold nanospheres electrostatically immobilized onto a Whatman paper, as miniaturized plasmonic transducers, with the synthetic RRWHRWWRR-NH2 polypeptide, as potent antimicrobial peptide, to obtain an efficient nanoplatform able to inhibit both the microbial activity and biofilm formation of two reference bacterial strains: *Staphylococcus aureus* ATCC 12600 and *Escherichia coli* ATCC 25922, respectively.

➤ The antimicrobial activity of the synthetic polypeptide specially RRWHRWWRR-NH$_2$– functionalized plasmonic paper on planktonic bacteria and biofilms was tested against two reference strains: Gram-positive bacteria *Staphylococcus aureus* (*S. aureus*) and the Gram-negative bacteria *Escherichia coli* (*E. coli*) determining microbial inhibition of up to 100% for planktonic bacteria.

➢ We fabricated three types of substrates using 500, 607 and 800 nm diameters at the beginning. Additionally, we used molecular- beam epitaxy (MBE) system to deposit 60 nm of silver nanoparticles on top of them. We also proved based on the results obtained through SEM and AFM images that the substrate 607 nm after silver particles deposition process attracted more our attention due its surface roughness marked by corrugation, nanometer-sized gaps, sharp apexes or ridges on top of the colloidal crystals indicating SERS-hot-spots presence.

➢ At the sight of the subtraction of *E. faecalis* from *E. coli*, the Raman spectrum resulting shows the specific peaks to *E. coli* positive values and *E. faecalis* negative values, while, the subtraction of 4-MPBA from each of them. The Results obtained show specific peaks to *E. coli* and *E. faecalis* all positive values. Given the fact that 4-MPBA molecule could probably give information about the eventual presence of both bacteria species but can discriminate or characterize the strains by our designed platform.

Future work implies the optimization of substrates' preparation and additional characterization on the samples with 4-MPBA. It would be interesting testing this approach and testing the feasibility to discriminate or clearly identify each bacterial strain.

REFERENCES

[1] **Hauptamann**. A., Klein. S., *Bronze Age gold in southern Georgia. ArcheoSciences.* 33, 75-82 (**2009**).

[2] **Warner** M. G., HUTCHISON J. E., *In Synthesis, Functionalization and Surface treatment of nanoparticles (Ed.M.-I. BARATON),* American Scientific Publishers: Stevenson Ranch, California, Chapter *5, p.* 67 (**2003**)

[3] **Giulio** F. P., David G. I. K., and Lawrence. T., *Colloidal Gold Nanoparticles: A Novel Nanoparticle Platform for Developing Multifunctional Tumor-Targeted Drug Delivery Vectors.* Drug Dev. Res. 67:47–54, (**2006**).

[4] Willets K. A., Van Duyne R. P., *Localized surface plasmon resonance spectroscopy and sensing.* Annual Review of Physical Chemistry, Annual Reviews, Palo Alto. 58, 267–297 (**2007**).

[5] Anker J. N., Hall W. P., Lyandres. O., Shah N. C., Zhao. J., Van Duyne R. P., *Biosensing with plasmonic nanosensor.* Nature Materials. 7, 442–453 (**2008**).

[6] Lin S.Y., et al., J. Phys. Chem. B 108, 2134 (**2004**).

[7] Kreibig. U. and Vollmer. M., *Optical Properties of Metal Cluster.* Springer, Berlin, (**1995**).

[8] Niemeyer C. M., *Nanoparticles, proteins, and nucleic acids: biotechnology meets materials science. Angew. Chem. Int. Ed.* 113 (22), 4128-4158 (**2001**). *Functional hybrid devices of proteins and inorganic nanoparticles.* Angew. Chem. Int. Ed. 42 (47), 5796-5800 (**2003**).

[9] Katz. E., Willner. I., *Integrated nanoparticle-biomolecule hybrid systems: synthesis, properties, and applications.* Angew. Chem. Int. Ed. 43 (45), 6042-6108 (**2004**).

[10] Katz. E., Shipway A. N., Willner. I., *Biomaterial-nanoparticle hybrid systems: Synthesis, proprieties and applications in Nanoparticles from Theory to Applications (Ed.: G. SCHMID), Wiley-VCH, Weinheim.* 368-421 (**2003**).

[11] Parak. W., Gerion J. D., Pellegrino. T., Zanchet. D., Micheel. C., Williams S. C., Boudreau. R., Le Gros M. A., Larabeil C. A., Alivisatos A. P., *Biological applications of colloidal nanocrystals.* Nanotechnology. 14 (7), R15-R17 (**2003**).

[12] Sak C. A., Maubach. G., Born. D., Reichert. J., Fritzsche. W., *DNA-based molecular nanotechnology.* Single Mol. 3 (5-6), 275-280 (**2002**).

[13] Penn S. G., Hey. L., Natan M. J., *Nanoparticles for bioanalysis.* Curr. Opin. Chem. Biol. 7 (5), 609-615 (**2003**).

[14] West J. L., Halas N. J., *Engineered nanomaterials for biophotonics applications: improving sensing, imaging, and therapeutics.* Annu. Rev. Biomed. Eng. 5, 285-292 (**2003**).

[15] Alivisatos A. P., *The use of nanocrystals in biological detection.* Nat. Biotechnol. 22, 47-57 (**2004**).

[16] Verma. A., Rotello V. M., *Surface recognition of biomacromolecules using nanoparticles receptors.* Chem. Commun. 3, 303-312 (**2005**).

[17] Antonii. F., *Panacea aurea-auro potabile. Hamburg: Ex Bibliopolio Frobeniano,* 250 (**1618**).

[18] Dreifuss**.** T., Barnoy. E., Motiei. M., Popovtzer. R., Bulte. J. Modo. M. *(eds.) Theranostic Gold Nanoparticles for CT Imaging In: Design and Applications of Nanoparticles in Biomedical Imaging.* Springer International Publishing, Cham, *pp.* 403-427 (**2017**).

[19] Dreaden E. C., Alkilany A. M., Huang. X., Murphy C. J., El-Sayed M. A., *The golden age: gold nanoparticles for biomedicine.* Chemical Society Reviews. 41 (7), 2740-2779 (**2012a**).

[20] Pietro G. G., Marc L. C., and Nathalie. L-G., *Handbook of Enhanced Spectroscopy*, (**2016**).

[21] Huang. X., Neretina. S., El-Sayed M. A., *Gold nanorods: from synthesis and properties to biological and biomedical applications*, Advanced Materials. 21, 4880–4910 (**2009**).

[22] Jana N. R., Gearheart. L., Murphy C. J., *Seed-mediated growth approach for shape-controlled synthesis of spheroidal and rod-like gold nanoparticles using a surfactant template*. Advanced Materials. 13, 1389–1393 (**2001**).

[23] Zheng.Y., Zhong X., Li. Z., Xia Y., *Successive, Seed-Mediated Growth for the Synthesis of Single-Crystal Gold Nanospheres with Uniform Diameters Controlled in the Range of 5–150 nm.* Particle & Particle. Systems. Characterizations. 31, 266-273 **2014**,

[24] Prevo B. G., O. D. Velev, *Controlled Rapid Deposition of structured Coatings from Micro-and Nanoparticle Suspensions*, Langmuir 20, 2099 (**2004**).

[25] Nikoobakht. B., El-Sayed M. A., J. Phys. Chem. A 107, 3372-3378 (**2003**).

[26] Nikoobakht. B., and El-Sayed M. A., *Preparation and growth mechanism of gold nanorods (NRs) using seed-mediated growth method.* Chem. Mater. 15, 1957, 62 (**2003**).

[27] Haidar. I., Aubard. J., Lévi. G., Lau-Truong. S., Mouton. L., Neuville D. R., Félidj N. B-L. L., *Design of stable plasmonic dimers in solution: importance of nanorods aging and acidic medium,* J. Phys. Chem. C. 58, 119 23149 (**2015**)**.**

[28] Jain P. K., Eustis. S., and El-Sayed M. A., *Plasmon coupling in nanorod assemblies: optical absorption, discrete dipole approximation simulation, and exciton-coupling model.* J. Phys. Chem. B 53, 110 18243(**2006**).

[29] Funston A. M., Novo. C., Davis T. J., and Mulvaney. P., *Plasmon coupling of gold nanorods at short distances and in different geometries,* Nano Lett. 8, 9 1651 (**2009**)**.**

[30] Mie. G., Beiträge zur Optik trüber Medien, speziell kolloidaler Metallösungen. Annalen der Physik. 330, 377–445 (**1908**).

[31] Bacalum. M., Janosi. L., Zorila. F., Tepes A.-M., Ionescu. C., Bogdan. E., Hadade. N., Craciun. L., Grosu. I., Turcu. I., et al., *Modulating short tryptophan- and arginine-rich peptides activity by substitution with histidine. Biochimica et Biophysica Acta (BBA)* - General Subjects, 1861, 1844–1854 (**2017**).

[32] Tsai T.-T., Huang T.-H., Chang C.-J., Ho N.Y.-J., Tseng Y.-T., Chen C.-F., *Antibacterial cellulose paper made with silver-coated gold nanoparticles.* Sci. Rep. 7, 3155 (**2017**).

[33] Zheng. Y., Zhong. X., Li. Z., Xia. Y., *Successive, Seed? Mediated Growth for the Synthesis of Single? Crystal Gold Nanospheres with Uniform Diameters Controlled in the Range of 5–150 nm.* Part. Part. Syst. Charact. 31, 266–273 (**2013**).

[34] Lantigua. D., Kelly Y. N., Unal. B., Camci-Unal. G., *Engineered Paper-Based Cell Culture Platforms.* Advanced Healthcare Materials. 6, 1700619 (**2017**).

[35] Pinto R. J. B., Marques P. A. A. P., Barros-Timmons A. M., Trindade. T., Neto, C.P. *Novel SiO2/cellulose nanocomposites obtained by in situ synthesis and via polyelectrolytes assembly.* Composites Science and Technology. 68, 1088–1093 (**2008**).

[36] Li Y. Q., Zhu. B., Li. Y., Leow W. R., Goh. R., Ma. B., Fong. E., Tang. M., Chen. X., Angew. Chem. Int. Ed. 53, 5837-5841(**2014**); Angew.Chem. 126, 5947-5951 (**2014**).

[37] Dimitrov A. S., Nagayama. K., Chem. Phys. Lett. 243, 462-468 (**1995**).

[38] Caldwell J. D., Glembocki O. J., Bezares F. J., Kariniemi M. I., Niinisto J. T., Hatanpaa T. T., Rendell R. W., Ukaegbu. M., Ritala M. K., Prokes S. M., Hosten C. M., Leskela M. A., Kasica. R., Opt. Express. **19**, 26056 (**2011**).

[39] Sau T. K., Rogach A. L., Jäckel. F., Klar T. A., Feldmann. J., Adv. Mat. **22**, 1805 (**2010**).

[40] **Li** Y. Q., Zhu. B., Li. Y., Leow W. R., Goh. R., Ma. B., Fong. E., Tang. M., Chen. X., Angew. Chem. Int. Ed. 53, 5837-5841(**2014**); Angew.Chem. 126, 5947-5951 (**2014**).

[41] **Moskovits**. M., Rev.Mod.Phys. 57, 783–826 (**1985**).

[42] **Otto**. A., Mrozek. I., Grabhorn. H., Akemann. W., J.PhysCondens.Mat. 4, 1143–1212 (**1992**).

[43] **Harz.** M., Rösch. P., Popp. J., *Cytometry*, Part A. 75, 104−113 (**2009**).

[44] **Kaisong**. Y., Qingsong. M., Xinjie. G., Youwei. X., Danting. Y., Beatriz J. S., Bingbing S., Chusheng. L., Ziwei. H., Guangchao. Y., Hongming. M., Hao. G., Christoph. H., Reinhard. N., Zhengjing. J., and Haibo. Z., *Antimicrobial peptide based magnetic recognition elements and Au@Ag-*

GO SERS tags with stable internal standards: a three in one biosensor for isolation, discrimination and killing of multiple bacteria in whole blood. Chem. Sci., 9, 8781 (**2018**).

[45] **Ankamwar**. B., Ujjal K. S., and Pulak. D., *SERS study of bacteria using biosynthesized silver nanoparticles as the SERS substrate.* Royal Society of Chemistry. Anal. Methods. **(2016).**

[46] **Kirchhoff**. J., Glaser. U., Bohnert. J. A., Pletz. M., Popp. J., Neugebauer. U., *Simple ciprofloxacin 389 resistance test and determination of minimal inhibitory concentration (MIC) within two hours using 390 Raman spectroscopy*. Anal. Chem. 90, 1811–1818 (**2018**).

[47] **Harz**. A., Rosch. P., Popp. J., *Cytometry,* Part A. 75, 104-113 (**2009**).

[48] **Kirschner**. C., Maquelin. K., Pina. P., Thi. N. A. N., Choo-Smith. L. P., Sockalingum G. D., Sandt C., Ami. D., Orsini. F., Doglia. S. M., Allouch. P., Mainfait. M., Puppels. G. J., Naumann. D., Journal of Clinical Microbiology. 39, 1763-1770 (**2001**).

[49] **Notingher.** I., Sensors. 7, 1343-1358 (**2007**).

[50] **Notingher**. I., Verrier. S., Romanska. H., Bishop A. E., Polak J. M., Hench L. L., Spectroscopy-an International Journal. 16, 43-51 (**2002**).

[51] **Puppels** G. J., Demul F. F. M., Otto. C., Greve. J., Robertnicoud. M., Arndtjovin D. J., Jovin T. M., Nature. 347, 301-303 (**1990**).

[52] **Huang**. Z., McWilliams. A., Lui. M., McLean D. I., Lam. S., and Zeng. H., *Near-infrared Raman spectroscopy for optical diagnosis of lung cancer*. InternationalJournal of Cancer, 107, 1047–1052 **(2003).**

[53] **Movasaghi.** Z., Rehman. S and Rehman I. U*., Raman Spectroscopy of Biological Tissues*, Applied Spectroscopy Reviews, 42, 5, 493 – 541 **(2007).**

LIST OF PUBLICATIONS

Papers published in ISI Journals

<u>Leopold Tie</u>, Monica Focsan, Jocelyne Bosson, Cristian Tira, Andreea Campu, Adriana Vulpoi and Simion Astilean, *Controlling the end-to-end assembly of gold nanorods to enhance the plasmonic response in near infrared*. Materials Research Express. 6 (**2019**) 095038.

<u>Leopold Tie</u>, Mina Raileanu, Mihaela Bacalum, Irina Codita, Stefania Madalina Negrea, CostinStefan Caracoti, Elena-Carmina Dragulescu, Andreea Campu, Simion Astilean and Monica Focsan, *Versatile Polypeptide-Functionalized Plasmonic Paper as Synergistic Biocompatible and Antimicrobial Nanoplatform.* Molecules. 25 (**2020**) 3182.

Paper in preparation

<u>Leopold Tie</u> et al., *Fabrication of SERS Substrates by Convective Assembly of Polystyrene Microspheres.*

Conferences

Controlling the end-to-end assembly of gold nanorods to enhance the plasmonic response in near infrared, **Leopold Tie,** Monica Focsan, Jocelyne Bosson, Cristian Tira, Andreea Campu, Adriana Vulpoi and Simion Astilean. The Sixth International Workshop on Advanced Nano- and Biomaterials and Their Device Applications French-Romanian Topical Meeting on Nano and Biomaterials "NABM 2019" Cluj-Napoca, Romania, 12th – 16th May 2019, **Oral Contribution.**

Designing Plasmonic Nanostructure for Biosensing Applications by Optical Spectroscopy, **Leopold Tie,** Alia Colniță, Daniel Marconi, Ioana Brezeștean, Lucian Barbu-Tudoran, Tiberiu Szöke-Nagy, Bogdan Cozar, Ioan Turcu, Simion Astilean and Monica Focsan. Conference of Doctoral Students from the University Consortium, 26-28 September 2019, Bucharest-Romania, **Oral Contribution.**

Controlling the end-to-end assembly of gold nanorods to enhance the plasmonic response in near infrared, **Leopold Tie,** Monica Focsan, Jocelyne Bosson, Cristian Tira, Andreea Campu, Adriana Vulpoi and Simion Astilean. The 15th Edition of International Conference on Analytical and Nanoanalytical Methodes for Biomedical and Environemental Sciences "IC-ANMBES 2018" Brasov, Romania, 23th -25th May 2018, **Poster Presentation.**

I dedicate my thesis first to my Lord, who has been and still be with me until to the end of this study.

I am thankful to Prof. Dr. Simion Aștilean who accepted me as a member of his excellent team. He really acted all his efforts towards me to provide facilities to do research in these fields of photonics and plasmonics. Beyond all these, he played his father's duty to me.

To Conf. Dr. Bosson Jocelyne, I am also grateful, she connected me to her colleague Prof. Dr. Simion Aștilean. All this took shape through her connection, I am very grateful to her.

I am thankful to CS I. Habil. Dr. Focșan Monica who assisted me in my work. She held my hands to go up by steps in this modern fields as a little child learns how to walk step by step. The expression of my deep gratitude to Prof. Dr. Mihai Todică and Conf. Dr. Dana Maniu for their sustained attention and contribution that they devoted to me.

I thank my colleague Dr. Andreea Câmpu for the helping hand, especially in the writing of articles and laboratory works. I thank all my colleagues, Dr. Monica Potara, Dr. Ana-Maria Crăciun, Dr. Timea Nagy-Simon, Dr. Sorina Suărășan, Dr. Sanda Boca-Farcău, Dr. Andra-Sorina Tătar, Drd. Raluca Ghiman, Drd. Raluca Borlan, Drd. Laurențiu Șușu, Drd. Alexandru Hada, may all know that each of them contributed a lot for my success.

I also thank my friends Drd. Jucan Darius, Drd. Isirabahenda Gonzague, Cornel, Dr. Popa Daniela, Dr. Ioan Botiz, Bogdan Marta, Drd. Cristian Țîra and family Zie and Toh bi for their encouragements, finances, and prayers support.

I am grateful to my spouse Mathilde Tie for the great patience, support and tolerating those times when I was always absent and i do not forget my pastors and all the church's members for all the things they did for me.

Last but not least, I have to thank my daddy and my mam for their support during the time of my university and their understanding for the little time I was able to spend with them when although being present, I was always absent because of my education.